MEASUREMENT OF THE NEUTRON PROTON SPIN CORRELATION PARAMETER A_{zz} AT FORWARD ANGLES

INAUGURAL DISSERTATION

zur Erlangung der Würde eines Doktors der Philosophie
vorgelegt der
Philosophisch-Naturwissenschaftlichen Fakultät
der Universität Basel

von

Hartmut Wöhrle

aus Deutschland

Basel 2006

Genehmigt von der Philosophisch-Naturwissenschaftlichen Fakultät auf Antrag von Prof. Dr. Ingo Sick und PD Dr. Jürg Jourdan

Basel den 16. Dezember 2003

Prof. Dr. Hans-Jakob Wirz

Acknowledgements

I thank my advisers Prof. Dr. Ingo Sick and PD Dr. Jürg Jourdan for the possibility to do this work. They allowed me to gain a lot of experience and learn a lot in various fields of experimental physics.

I also want to thank the members of the group who helped me with my experiment. We walked together on a very interesting, enlightening and inspiring way. Also I'd like to thank all of our postdocs who gave me a hand to look into the right direction.

It was a pleasure to work with all these bright people.

Very warm thanks go to my mother and my sister for their support and their help. And especially to my father who always believed in me but wasn't able to see the end of my work - I miss you.

— "Es gibt eine Theorie die besagt, wenn jemals irgendwer genau herausfindet, wozu das Universum da ist und warum es da ist, dann verschwindet es auf der Stelle und wird durch etwas noch Bizarreres und Unbegreifliches ersetzt"
— "Es gibt eine andere Theorie, nach der das schon passiert ist."
Douglas Adams, "Das Restaurant am Ende des Universum"

Abstract

The n-p spin correlation parameter A_{zz} was measured at an energy of 68 MeV and 7 angles in the range of $22.5^o - 57.3^o$ CM with a statistical accuracy better than 0.01.

In the measured range, A_{zz} is most sensitive to ϵ_1, the mixing parameter of the deuteron states $^2S_1$ and $^2D_1$. Therefore the measurement is expected to reduce significantly the uncertainties of the phases in the energy range below 100 MeV, when a new global Phase Shift Analysis (PSA) is performed. This should help to find a more accurate answer to the strength of the tensor force in the NN-interaction.

The experiment was performed in the low energy area C (NEC) of the Paul Scherrer Institute (PSI) in Villigen, Switzerland.

Contents

List of Figures

List of Tables

1 Theory

1.1 Introduction

The nucleon – nucleon interaction at low energies can be described via the exchange of mesons. Nucleon – nucleon potentials derived from meson theory contain the tensor force term which represents one of the most important parts.

The accurate knowledge of the tensor force is essential for the understanding of the structure of nuclear systems. For example the D-state of light nuclei (A=2,3) or the non-vanishing quadrupole moment of the deuteron are a direct consequence of the tensor force.

One effect of the tensor force is the mixing of states with different angular momentum ($L = J \pm 1$, J=total angular momentum). This mixing can be described with mixing parameters ϵ_i in a phase-shift-analysis (PSA) of nucleon – nucleon scattering data.

The lowest order mixing parameter ϵ_1, which is most relevant in the energy regime of nuclear structure calculations ($^{k_F^2}/_{2M}$ ≈35MeV, k_F = Fermi Momentum), describes the mixing between $^3S_1$ and $^3D_1$ states with lowest angular momentum L=0,2 . Until today the knowledge of ϵ_1 is unsatisfactory.
As one can see in figure 1 the world database on values of ϵ_1 from single — energy phase shifts does not agree with predictions of meson exchange potentials, but the errors of the existing PSA data are too large to provide a sufficient constraint. The values of ϵ_1 a given by the various modern potentials (Paris[15], Bonn[16], Nijmegen II[17], Argonne v18[27]) are lower than the world data presently available. This would indicate a stronger tensor force than given by the fits, in particular in the region between 50 and 130MeV.

An increase of the accuracy of ϵ_1 is only possible with precise measurements of higher order spin observables [12], such as spin correlation parameters and spin

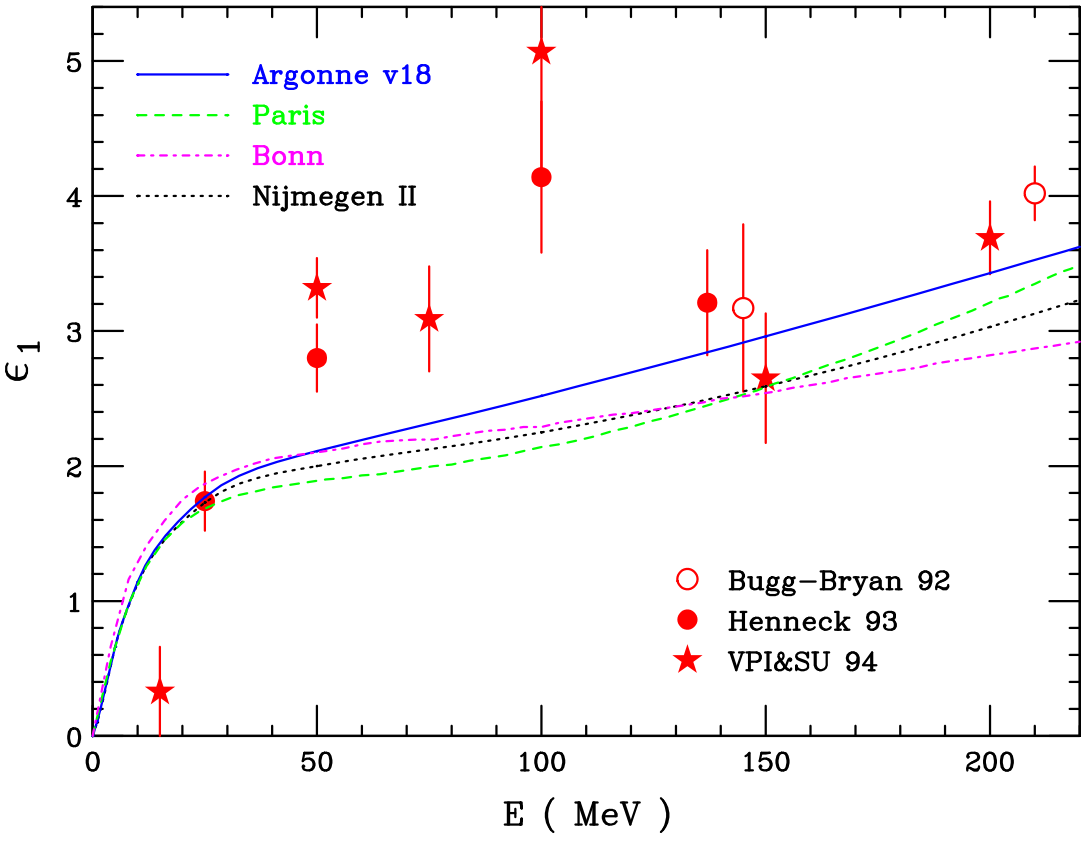

Figure 1: World data on ϵ_1 and some predictions from different potential models

dependent total cross sections. Such observables are difficult to measure, because both beam and target have to be polarized. In addition, the observables sensitive to ϵ_1 are in general also sensitive to the poorly known $^1P_1$ phase. As shown in the analysis by Binstock and Bryan [26] the observable most sensitive to ϵ_1 is the spin correlation parameter A_{zz}.

In figure 2 the data of former experiments [1, 19] at 68MeV are plotted in comparison to the result of a PSA by Henneck[20]. Also included are the PSA results for variations of ϵ_1 by $\pm 1^\circ$ and variations of $^1P_1 \pm 1^\circ$.

The experimental data by Hammans[19] in the backward angular range show small errors because at backward angles the energy of the recoil proton is large enough to escape the target so the proton can be detected. But the influence of

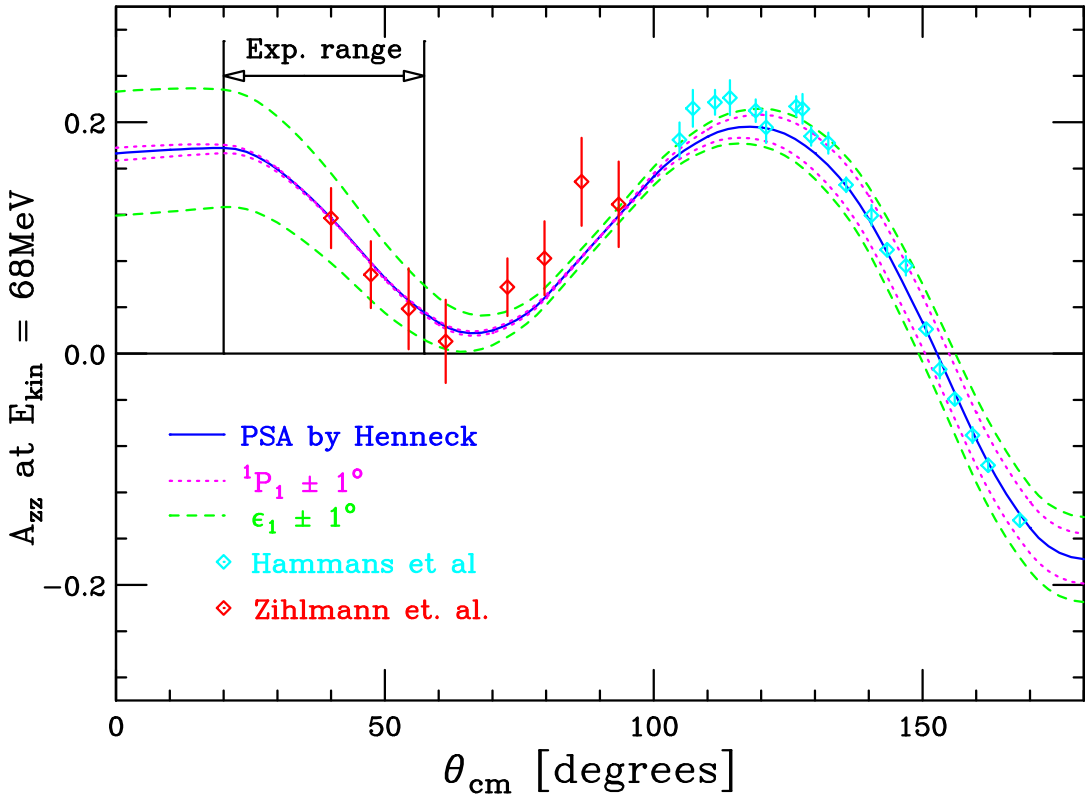

Figure 2: A_{zz} from a PSA by Henneck and data of previuos experiments. Also shown is the angular range (CM) of the present experiment

$^1P_1$ on the value of A_{zz} is strongest in this area and is of the same order as the potential variations of ϵ_1. This correlation limits the accuracy by which ϵ_1 can be determined from such a measurement.

The forward angular range covered by the data of Zihlmann[1] should allow for a more accurate determination of A_{zz} because in this range the influence of $^1P_1$ nearly disappears. Especially at scattering angles from 40° to 80°deg in the *center of mass* (CM) a variation of ϵ_1 shows a larger effect upon the value of A_{zz}.

However, from the experimental point of view, data in the forward angular range are not as easy to measure. In the forward angle range, the energy of the proton is too small to let the photon escape from the target. Therefore every experiment in the forward angular range has to detect the neutron. Detecting the neutron

is only possible by an indirect process, because most detection methods require a charged particle, that is able to ionize or excite the detector material. In the experiment of Zihlmann the detection of the neutron was done in a detector consisting of an array of plastic scintillators.

In addition, the differential cross section for scattering from ^{12}C and ^{16}O in the (typical Butanol–) target increases in the angular range to a value of up to 100 times the one for hydrogen scattering. These two experimental problems increase the background and complicate the identification of the interesting events. While the data from Zihlmann in the forward angular range (40°-60°CM) seem to confirm the A_{zz} values derived from the PSA, they can not place restrictive constraints on ϵ_1.

Due to progress in developing a polarizable target that consists of a piece of *scintillating* plastic, it is now possible to extend the range of precise experimental data to the very forward angular range.

A scintillating target allows one to detect the recoil proton within the target and perform a coincidence measurement between the signal from the target and a neutron detector placed in the desired angular range. With such a coincidence it should be possible to eliminate – or at least identify and subtract in a later analysis – the background. This experiment was only possible with the introduction of this target type (described in sec.10 p.13) and the work performed for this thesis also contributed to the target development (described in sec.2.1 p.6).

1.2 Formalism

For spin $^1/_2$ on spin $^1/_2$ scattering the formalism described in appendix A is extended so that the initial state, which is described by the density matrix, now consists of a product of the density matrices for beam and target. Its constituents are permutations of products of the polarization and the spin (Pauli matrices) of

beam and target in the 3 spatial directions (x,y,z)

$$\rho_i = \rho_{beam} \otimes \rho_{target} = \frac{1}{4} \sum_{j,k=x,y,z} p_j^b p_k^t \sigma_j^b \sigma_k^t \tag{1}$$

with the upper indices b = beam and t = target. The differential cross section is proportional to the trace of the final density matrix.

$$\frac{d\sigma}{d\Omega} \propto Tr(\rho_f) \tag{2}$$

It consists of a sum of products of beam and target polarizations and the spin correlation parameters. One of them is the term A_{zz} we are interested in.

$$\frac{d\sigma}{d\Omega} = \frac{d\sigma_0}{d\Omega}(1 + p_y^b A_y^b + p_y^t A_y^t + \cdots + p_z^b p_z^t A_{zz}) \tag{3}$$

When beam and target are polarized in z- or *in-flight*-direction the other terms disappear and there is only one remaining

$$\text{Spin parallel: } \frac{d\sigma}{d\Omega}(\uparrow\uparrow) = \frac{d\sigma}{d\Omega}(\downarrow\downarrow) = \frac{d\sigma_0}{d\Omega}(1 + p_z^b p_z^t A_{zz}) \tag{4}$$

$$\text{Spin antiparallel: } \frac{d\sigma}{d\Omega}(\downarrow\uparrow) = \frac{d\sigma}{d\Omega}(\uparrow\downarrow) = \frac{d\sigma_0}{d\Omega}(1 - p_z^b p_z^t A_{zz}) \tag{5}$$

When solving the equations for A_{zz} one obtains the relation to the asymmetry measurement of cross sections for the different spin states

$$measured\ asymmetry = \frac{\frac{d\sigma}{d\Omega}(\uparrow\uparrow) - \frac{d\sigma}{d\Omega}(\downarrow\uparrow)}{\frac{d\sigma}{d\Omega}(\uparrow\uparrow) + \frac{d\sigma}{d\Omega}(\downarrow\uparrow)} = p_z^b p_z^t A_{zz} \tag{6}$$

For the experimental analysis, the equation can be expressed by an asymmetry of counted events

$$measured\ asymmetry = \frac{N(\uparrow\uparrow) - N(\uparrow\downarrow)}{N(\uparrow\uparrow) + N(\uparrow\downarrow)} = p_z^b p_z^t A_{zz} \tag{7}$$

2 Target development

2.1 Target

As mentioned in the introduction, a former experiment [1] in the angular range of 40° – 93.5° CM indicated that the forward angular range becomes extremely sensitive to neutron–carbon scattering. In the region of $46°_{lab}$ – $19°_{lab}$ the differential cross section for n–^{12}C scattering rises from 5 to 500mb/sr, compared to a rise from 20 to 40mb/sr for n–Hydrogen scattering. Thus one expects that it will be hard or nearly impossible to measure with a similar setup as used in [1] at the very forward scattering angles. Only an experiment with the possibility to identify and separate n–^{12}C and n–Hydrogen scattering can provide significant data for A_{zz}.

Together with the polarized target group of PSI[1], the development of a so called *active polarizable proton target*, made from polarizable plastic scintilators, became the first and most important part of this experiment. During the preparation of the setup — including several beam times at PSI — we started target tests with the Cockcroft-Walton accelerator in the Institute of Physics in Basel.

2.2 Active proton target

The goal for the present experiment was to develop a $18mm \times 18mm \times 5mm^3$ polarizable plastic scintillator to be used as an active target.

This target consists of a Bicorn BC400 scintillator material, treated with TEMPO (based on different types of 2,2,6,6 – methyl – piperidine – 1 – oxyl: $C_9H_{18}NO$ / $C_{11}H_{20}NO_3$ / $C_{12}H_{21}N_2O_2$, see [24]) which contain a free radical. This chemical solution is a dark brown liquid. After testing several methods in producing the target without destroying the scintillation properties or the polarization capacity,

[1] Paul Scherrer Institute, Villigen, Switzerland

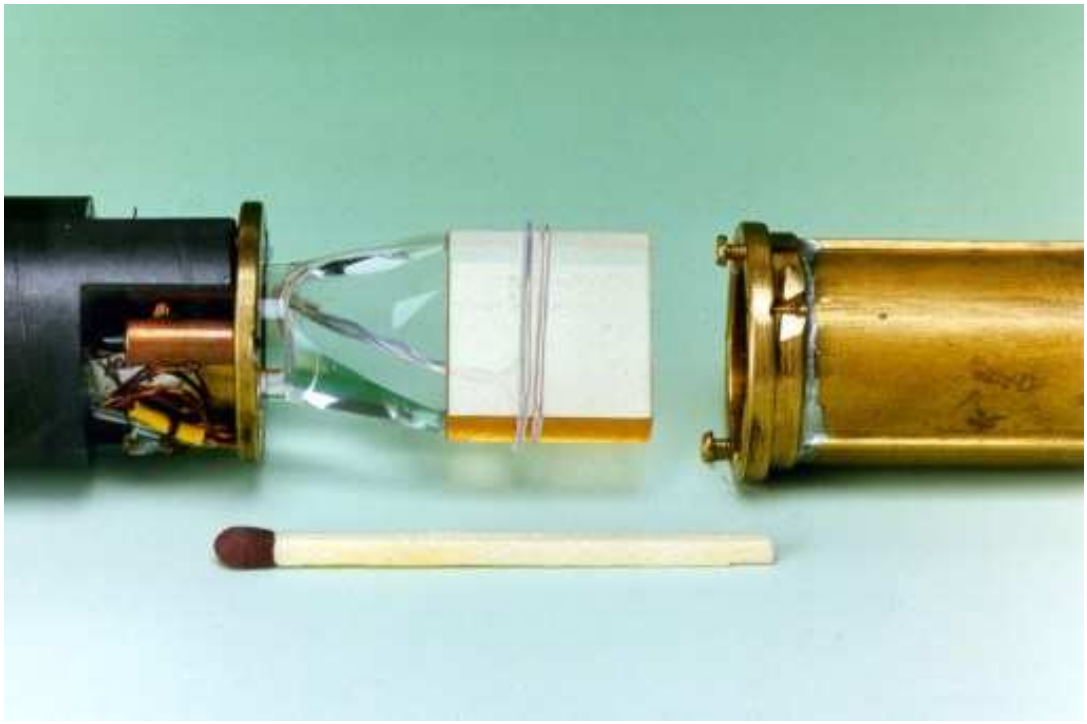

Figure 3: Sample of the polarizable active target and the NMR coil, mounted on the lower end of the PSI dilution refrigerator [18]

the preparation by dissolving the scintillator, adding the free radical and pressing the resulting 0.1mm films at temperatures of 100°C to 130°C (the various production trials and results can be found at [21]) turned out to be best. The resulting slightly brown solid block of $18mm \times 18mm \times 5mm^3$ was polished to get surfaces with better light reflection.

This solid block can be polarized by dynamic polarization. This is done in a strong magnetic field ($\sim$ 2.5T) which defines the polarization direction, by inducing with microwave radiation spin-flips of the protons; this is done at $\sim$2–3K as described in [5] and [18].

The target was glued to a crystal fishtail attached to a 100cm plastic light guide with a diameter of 12mm. On top of the light guide a photomultiplier records the transmitted light. The photomultiplier is shielded against the magnetic field

with a cover of μ-metal.

2.3 Test setup

An incoming ^{3}He beam with an energy of 1.34MeV hits a deuterium gas chamber with a length of 18cm. After passing the 2μm Al foil entrance window the remaining energy of the ^{3}He is around 1MeV. Depending on the place of the $D(^3He, p)^4He$- reaction, the proton energy is 18.5 – 19.5MeV. After passing the exit window, a 300μm Al foil, we have a proton energy of $\sim$ 18MeV. To reduce the energy to $\sim$ 3MeV, which is the minimum energy used in the experiment at PSI, we place an undoped BC400 scintillator with a thickness of 3mm in front, 6cm from the exit of the gas chamber. This scintillator also provides the start signal for the electronics.

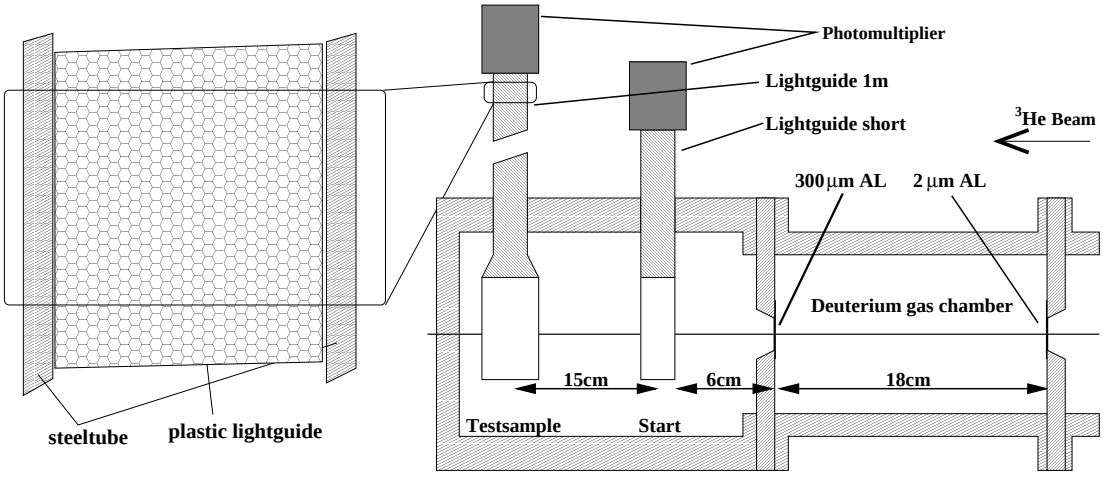

Figure 4: Setup for the target tests

Above the scintillator, a short (10cm) light guide with a photomultiplier on the topside is mounted. In the back, at a distance of 15cm, is placed the test sample with a 1m light guide and a photomultiplier at the end. The setup for the test sample with the 1m light guide is similar to the one used in the experiment later. The light guide is a plastic tube with a diameter of 12mm. The coupling between light guide and sample is done by a fishtail like plastic to change between

the rectangular sample and the circular light guide. The target chamber was evacuated and at room temperature.

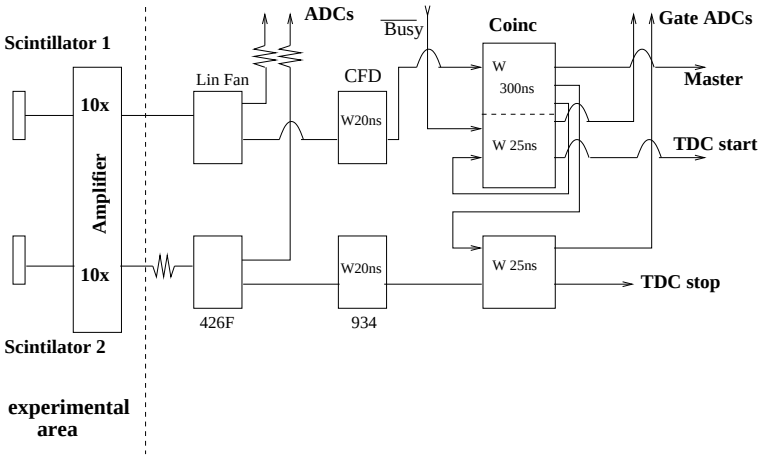

Figure 5: Electronics setup for the target tests

The front scintillator was not only used to decelerate protons to the desired energy range, but also to suppress background. The electronic setup uses the signal the two scintillators in coincidence. Scintillator 1 gives the start signal, opening a gate of 300ns for the electronics and a gate of 25ns for the ADC and TDC acceptance. Scintillator 2 provides the stop signal for the TDC.

2.4 Target tests

Test measurements include a calibration measurement with an untreated BC400 scintillator of the same dimensions as the target samples. All sample measurements were compared with this reference. With the described setup it was possible to test various targets under the same conditions as used in the experiment. The target with the best time and energy resolution was selected for the experiment.

While developing the target setup, tests with coated light guides were also carried out, in order to improve the internal reflection of the scintillation light at the

surface of the light guide in direction towards the photomultiplier and increase the light output. It turned out that this coating - black paint and aluminum - absorbs more light than an uncoated light guide within a polished tube. This is mainly because one can not avoid the surface being scratched while inserting the light guide in the tube. The light that is diffracted to the outside of the coating is not able to be reflected back inside, so this part of the scintillator light is lost. In the final experimental setup the inner surface of the steel tube was polished and the light guide left untreated.

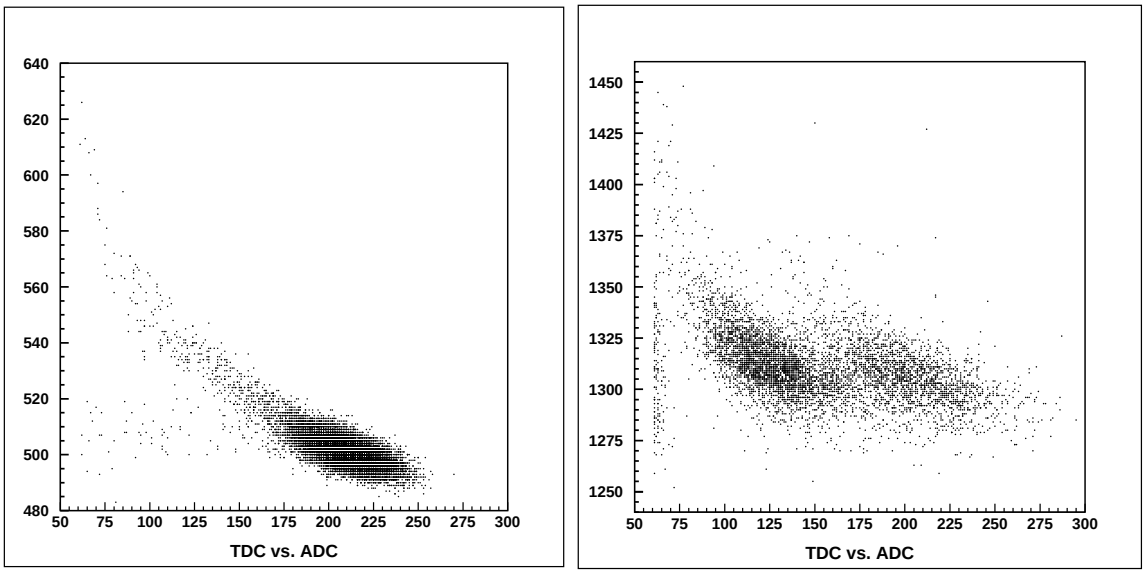

Figure 6: Reference and sample used in August experiment

3 Experiment

3.1 Experimental setup

This experiment is a so called *double-polarization* experiment which means that both beam and target are polarized. The experiment makes use of the *low energy experimental hall C* (NEC) at PSI. The atomic ion source [6] produces transversally polarized protons which are injected into the Phillips Cyclotron and accelerated to a beam energy of 71MeV. The radio frequency is 50.6 MHz. Thus every 20 ns a beam bunch is extracted.

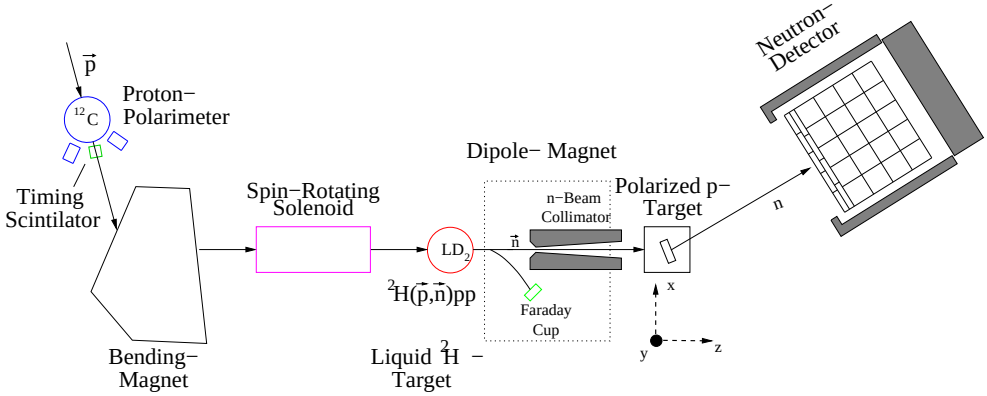

Figure 7: Experimental setup at PSI (NEC)

When the beam enters the hall, the polarization of the beam is measured with a ^{12}C polarimeter (see section on proton polarization p.17) and the time structure is measured with a timing scintillator placed 30° below the beam line.

In a right handed coordinate system with the z-axis parallel to the beam direction the spin of the proton beam is parallel to the y-axis. This is the spin orientation when entering the hall and when passing the ^{12}C polarimeter.

After the last bending magnet, the magnetic field of a spin rotating solenoid turns the proton spin of the beam from the y to the x direction orthogonal to the beam direction. Then the beam hits a liquid deuterium target of 1cm thickness and 2cm

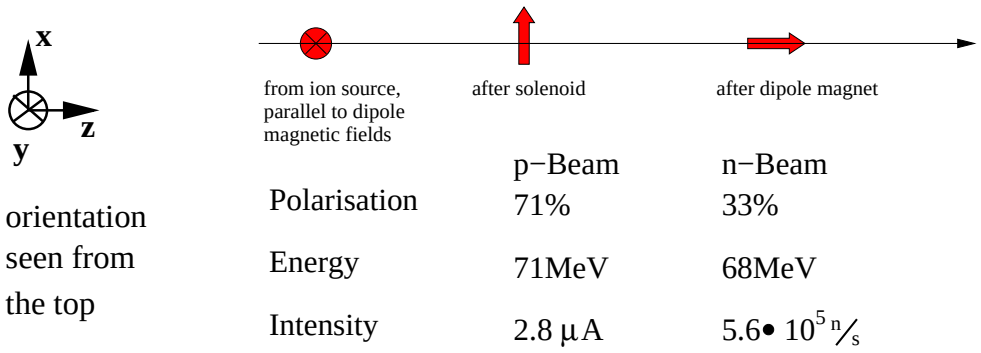

Figure 8: Average spin and beam properties at the NEC (PSI)

diameter [25]. Here the neutron beam is produced via the ${}^2H(\vec{p},\vec{n})pp$ reaction at zero degrees. Right in front of the target a *secondary electron emission monitor* (SEM) is placed. It consists of a set of 4 havar foils which cover the left, right, upper and lower halves of the beam cross section, leaving a gap of 2×2mm. If the beam moves out of the center, one or two of the foils detect an increased current. With this information a feedback loop program uses the steering magnet before the SEM to compensate until the currents are equal. The dipole magnet behind the deuterium target has two functions: on the one hand it bends the remaining protons to the Faraday cup to measure the beam current; on the other it turns the neutron spin from the x to the z (in–flight) direction (see [4] for a detailed discussion). After the liquid deuterium target a brass collimator of 1.5m length reduces (see [25] for a detailed discussion) the neutron beam to a 2cm spot when hitting the polarized active target.

3.2 Active Target Setup

At a distance of 3m downstream of the neutron target, the proton target toploading cryostat containing the active target is placed. It consists of the target holder, including all required supplies for cooling, microwave, NMR and a set of Helmholtz coils to generate a magnetic field for the target. The construction is described in [18].

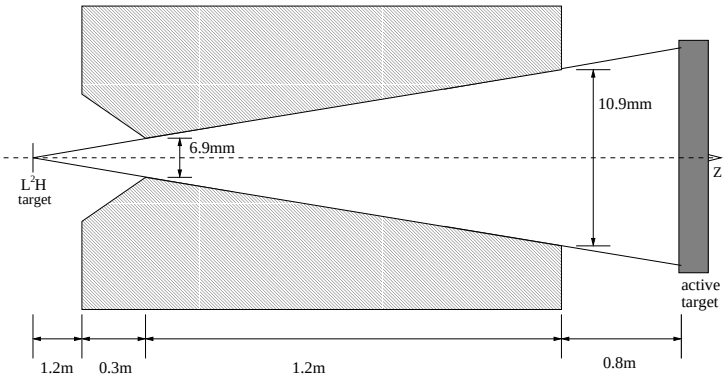

Figure 9: Brass collimator used in NEC (PSI)

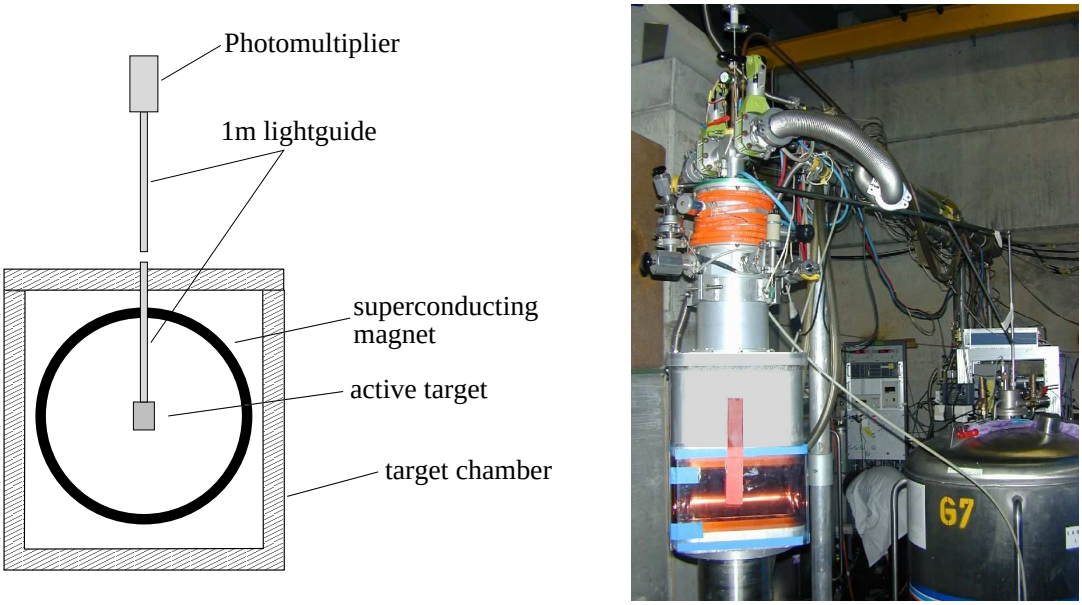

Figure 10: Target schematic drawing and photograph of setup

After reaching the highest polarization the target polarization is frozen by lowering the temperature to $\sim$ 100mK by using a ^{3}He – ^{4}He dilution refrigerator as described in [18]. At this temperature the magnetic field can also be lowered to a less strong holding field and the microwave generator can be switched off, as described in [22] and [23]. At the temperature of 90mK and a holding field of 0.4T the relaxation time of the target is 70h; when using 0.8T the relaxation time is increased to 240h [21].

The target polarization is measured every 10min with a NMR coil wound around

the target scintillator (as can be seen in figure 3) and reaches the average values mentioned in table 7. From the integral over the NMR signal, the target group can calculate the target polarization when using the thermal polarization (no microwaves) for calibration. The errors of the polarization determination are mainly due to the systematic uncertainty of the temperature measurement at such low temperatures.

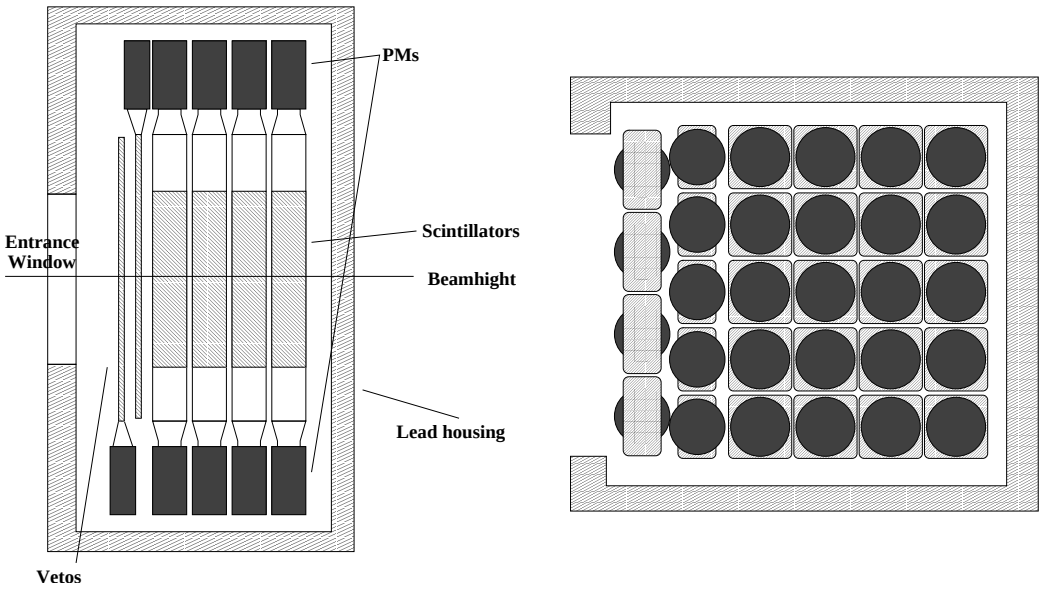

Figure 11: Schematic drawing of the neutron detector, top and side view.

3.3 Neutron Detector

The neutron detector consists of 20 plastic scintillator bars ($50cm \times 10cm \times 10cm$) arranged in 5 columns and 4 rows, each of them with PMs on both sides. In other experiments with charged particles at the MAMI accelerator in Mainz, the time difference between the signals of the upper and lower PM is used to extract the vertical position of the event. But in the present experiment the position information was not used. In front of the bars, there are 9 thin (1cm) scintillators, which are used as veto for charged particles.

The detector is surrounded by a lead house of 2 layers with 5cm thickness each

and a total weight of 10tons. The house has an entrance window facing the target, which can be closed by thin lead plates when used in other experiments at higher energies. In the present experiment with low energy neutrons and protons it was not necessary to use this shielding. In addition, the back is left open for better handling of the cables, but shielded with a concrete block.

3.4 Positioning

The target is placed on top of a stand that is screwed to the hall floor. This is a permanent installation at the NEC and has been surveyed with an accuracy of about 1mm. With a set of three screws the stand can be adjusted in the vertical direction to an accuracy of 1mm. Then the cryostat housing is placed on top of the stand and the target scintillator turned to face the neutron detector.

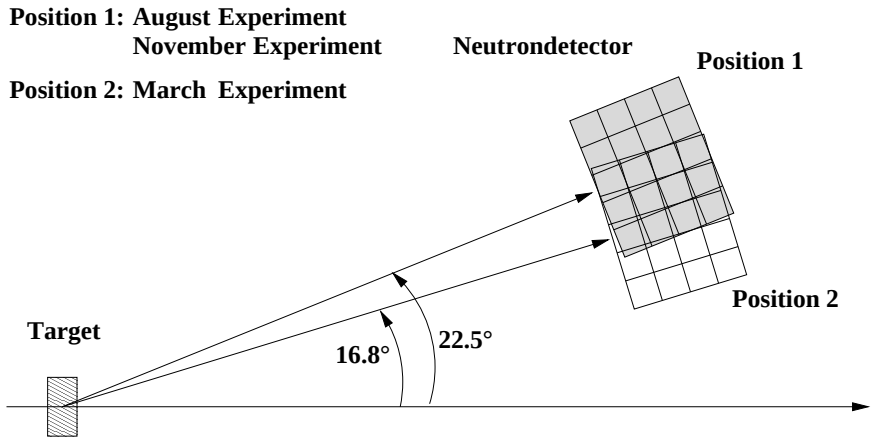

Figure 12: Position of the neutron detector for the different run times

The beam line is at a height of 156cm above the hall floor. The center of the target and the neutron detector is mounted at this height. In 3 experimental runs the neutron detector is placed at a distance of 200cm from the target at 2 center angles: $16.8°_{lab}$ (August 1998 and November 1998) and $22.5°_{lab}$ (March 1999) as shown in figure 12, with overlapping angular range. With this arrangement we cover a total range of 7 angles from $28°_{lab}$ to $11°_{lab}$ ($56°_{CM}$ to $22°_{CM}$).

At the 16.8°$_{lab}$ angle, the innermost edge of the detector lead shielding is ∼10cm away from the beam line. At this distance the beams spot has a diameter of 4cm.

3.5 Electronics setup

In this experiment we need to handle 49 signals from the neutron detector, 1 from the target and 5 signals from the usual setup in NEC (2×polarimeter, timing scintillator, Faraday cup, accelerator RF).

For each event, the incoming signals are treated in two ways: on one hand they are used for the determination of the energy and on the other hand for the measurement of the time. In addition a trigger signal is generated.

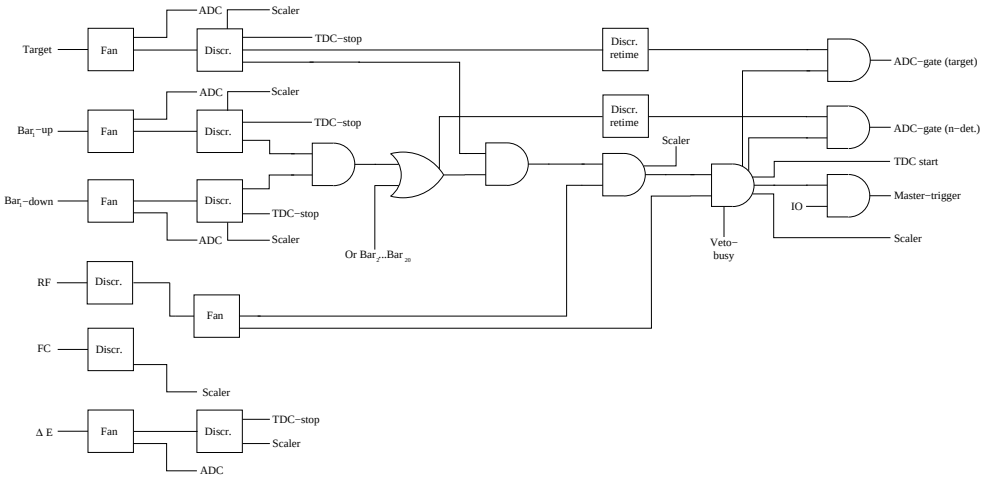

Figure 13: Electronics setup

First the incoming signal is distributed with a linear fan to an *analog-to-digital* converter (ADC) and a discriminator module. The ADC integrates the signal amplitude which is proportional to the energy deposited in the plastic. The other output of the fan is fed into a *constant fraction discriminator* (CFD), which creates a logic signal with a time independent of the signal amplitude. The discriminator output provides signal for a scaler, the *time-to-digital* converter

(TDC) stop signal, a second discriminator and a coincidence with the neutron detector.

At this point the detector and the target signals are treated a little differently. For each bar of the neutron detectors a coincidence of the upper and lower PM is performed. A logical OR combines all bars to one neutron detector trigger signal.

Now this signal and the logic signal of the target are fed to a logical AND to detect the target–detector coincidence, which allows to suppress most of the background. The output signal is fed into a coincidence unit together with the cyclotron RF which defines the timing of the output signal. The output is used for the TDC start, a scaler and for the master trigger. A *computer-busy* is taken into account to reject events while the electronics is busy.

An additional discriminator in all signal lines gives a re-timing of the event, to provide the ADC gates at proper time. These gates are 42ns wide for the neutron detector and 50ns for the target. While every 20ns a beam bunch reaches the hall, it is possible that events from a previous or following beam bunch are accepted accidentally as shown in figure 16.

The signals from the 9 ΔE scintillators in front of the neutron detector are accepted and given to an ADC and scaler but not taken into account in the logic chain.

3.6 Proton polarization

The proton beam polarization was measured using a ^{12}C polarimeter with a $200\mu m$ carbon foil and 2 NaI detectors located at 44°. At this angle the analyzing power for the $^{12}C(\vec{p},p)^{12}C$ elastic scattering is maximal[7][8] and known with a precision of $\pm 0.1\%$.

The signals of the NaI crystal detectors are amplified and combined with a pulser signal. This is recorded by an ADC the output of which is stored within a

Borer-Buffer module. The pulser is also fed into a scaler, and used to correct for dead time of the electronics. In addition, the scaler signal can be used as a normalization of the spectrum.

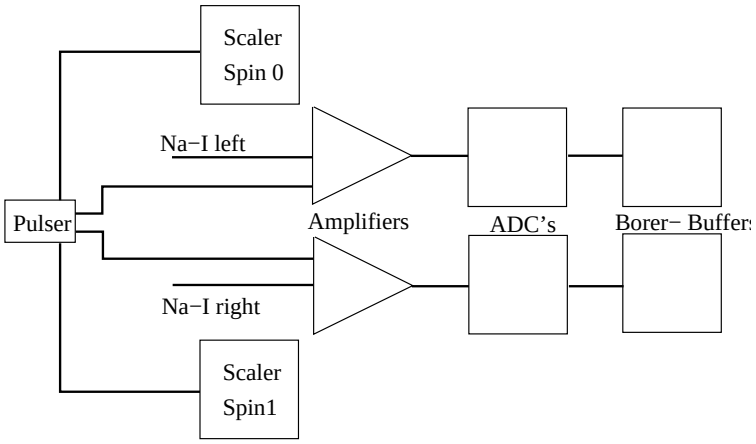

Figure 14: Polarimeter electronic setup

The Borer–Buffers generate an ADC spectrum which allows to discriminate between the ^{12}C ground state and the excited states. For the following only the elastic scattering rate is used. Due to the spin – orbit coupling there is an asymmetry in the scattering to the left and the right detector

The analysis uses the so called *super ratio method* to avoid effects caused by beam asymmetries

$$P_{\vec{p}} \cdot A_y = \frac{\alpha - 1}{\alpha + 1} \quad \text{with} \quad \alpha = \frac{N_l^{\uparrow} \cdot N_r^{\downarrow}}{N_l^{\downarrow} \cdot N_r^{\uparrow}} \quad \text{and} \quad A_y = 0.9864 \pm 0.0010 \tag{8}$$

The resulting proton polarization calculated by this method is the average of the two polarization states ($P_{\vec{p}} \uparrow$ and $P_{\vec{p}} \downarrow$). As one can see in the histograms figure 19 the overall variation of the beam polarization is in the range of 2-3%. But within a run set the variation is less than 1%, so I can assume an average beam polarization for every *run-set*.

As shown in the section about corrections page 26 there is a difference between intensity of the proton beams for the two polarization states. When looking at the spectra of one polarimeter detector figure 15 one observes a slight shift in the peak position. This shift appears at the November and March beam times, but not in August. The effect of this shift is the reason for a correction introduced on page 27

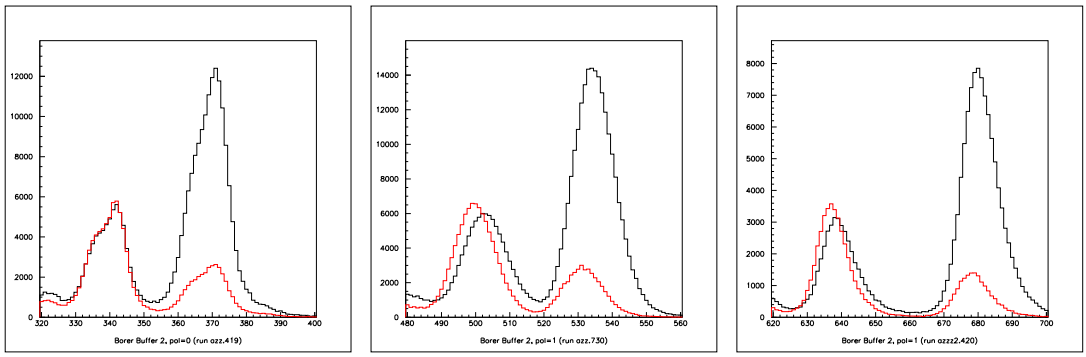

Figure 15: Polarimeter spectra for August, November and March beam time. $P_{\vec{p}} \uparrow$ (black) and $P_{\vec{p}} \downarrow$ (red) of the same detector

3.7 Neutron polarization

The neutron production facility is a permanent installation in the NEC which was used for several years by our group. It includes a liquid deuterium target where the neutrons are produced by the breakup reaction $d(\vec{p},\vec{n})pp$ at 0°. The neutron spectrum at 0° is almost mono energetic [10] and the spin transfer is of the order of 50% but dependent on the energy of the neutron [11].

The spin transfer ratio of the breakup reaction at the energy range of this experiment (around 70MeV) was calibrated to a high precision in [3], [2]. For this experiment at a proton enery of 71MeV the value is $K_y^{y'} = 0.4575 \pm 0.0051$.

The polarization of the neutron beam is calculated via:

$$P_{\vec{n}} = K_y^{y'} \cdot P_{\vec{p}} \tag{9}$$

4 Analysis

4.1 Data analysis

The main information on the scattering events is contained in the target TDC and ADC spectra. These data are used to obtain the count rates for the analysis. Because of the coincidence setup of this experiment (see electronics setup p.16), the analysis is mainly based on the TOF signals of the neutron detector in relation to the signal from the target. With this information it is possible to identify much of the background and accidental events as shown in figure 17. In addition, most of the background is suppressed by the hardware coincidence leading to a much better *signal to background* ratio than in the usual single arm experiment.

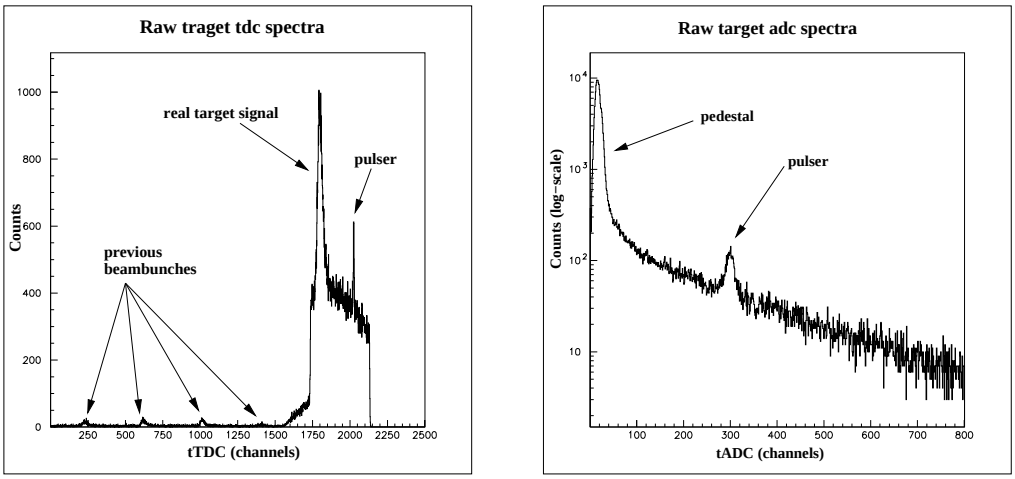

Figure 16: Raw target spectra

In order to identify n-p elastic scattering events the first cut is done on the veto detectors to eliminate charged particles. Next is the cut on the target TDC (figure 16 left), which selects the *time of flight* from the accelerator to the target and the cut of lower channels of the target ADC (figure 16 right), which reduces electronic noise and low energetic background.

The most important information is the *time-of-flight* between target and neutron

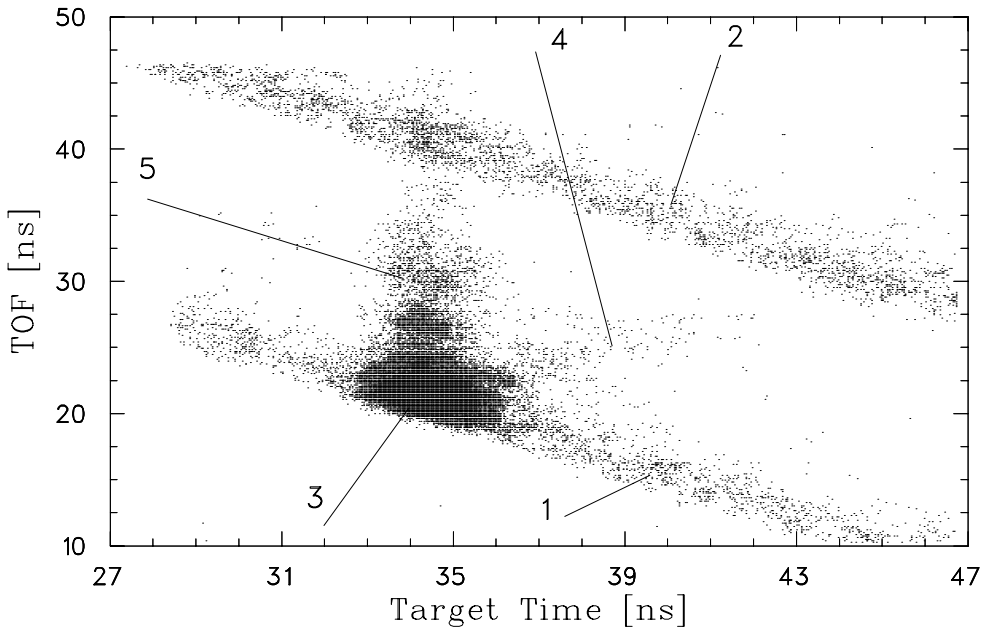

Figure 17: Target TDC versus time-of-flight for one bar of the neutron detector

detector. Here we can cut in a two-dimensional time histogram of target versus each neutron detector bar.

Figure 17 shows a two dimensional plot of target time versus *time of flight* between target and one neutron detector bar. In this histogram one can identify the desired scattering information, marked as 3, and separate it from accidental events, marked as 1 (same beam bunch) and 2 (previous beam bunch). Also n-p elastic scattering from slower neutrons, marked as 4 and the problematic n–^{12}C scattering, marked as 5, can be identified. The remaining background under the signal peak (3), which comes mainly from the accidentials marked as (1), is less than 30% of the real signal and can be extracted as will be discussed on page 28.

When summing up the events in the target ADC with respect to an angular row of the neutron detector we obtain the count rates for each angle, while the raw target ADC spectrum figure 16 is separated in the five spectra as shown in figure 18.

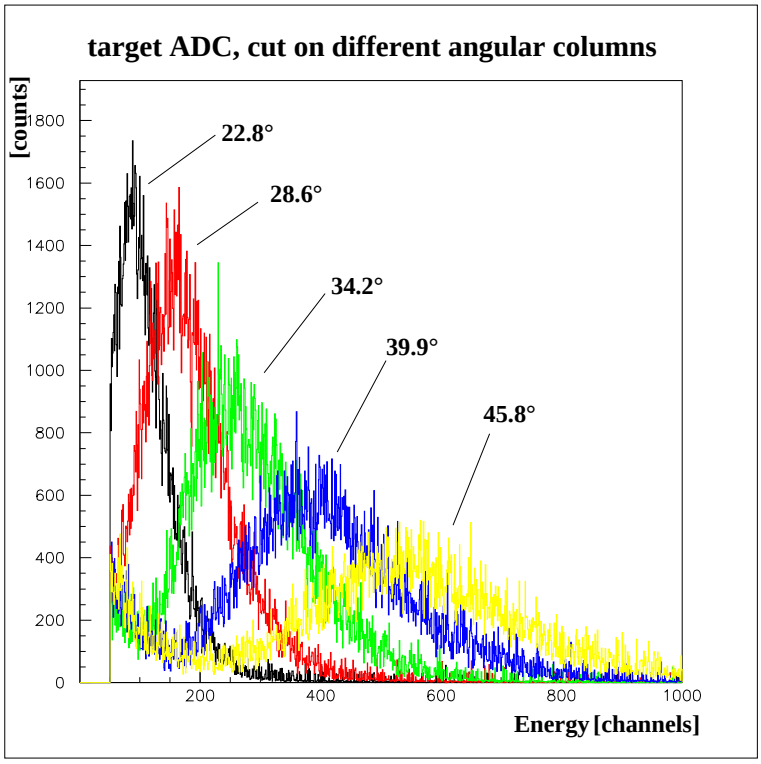

Figure 18: Target ADC with cut on different angles of the neutron detector

4.2 Beam polarization

As mentioned in the schematic overview of the experimental setup, the incoming beam is a y-direction polarized proton beam. The proton spin is turned into the x-direction using a solenoid with a magnetic field in z-direction. The orientation of the field can be switched to *in flight* or *against flight* direction. This is done several times during the experiment to cancel systematic asymmetries. So we have a set of combinations describing the magnetic field direction of solenoid and target. These combinations give a total of 13 sets which are listed in table 6. If, in the following, a *run set* or *data set* is mentioned, refer to this table.
The incident spin direction of the source is switched every 3 seconds. This switching is part of the polarization measurement and the extraction of the A_{zz} asymmetry, but does not count in this table.

The average proton beam polarization is measured for every run as described on page 17. There are some fluctuations during the experiment as can be seen in figure 19, but they are small and within a set of runs usually less than 1%.

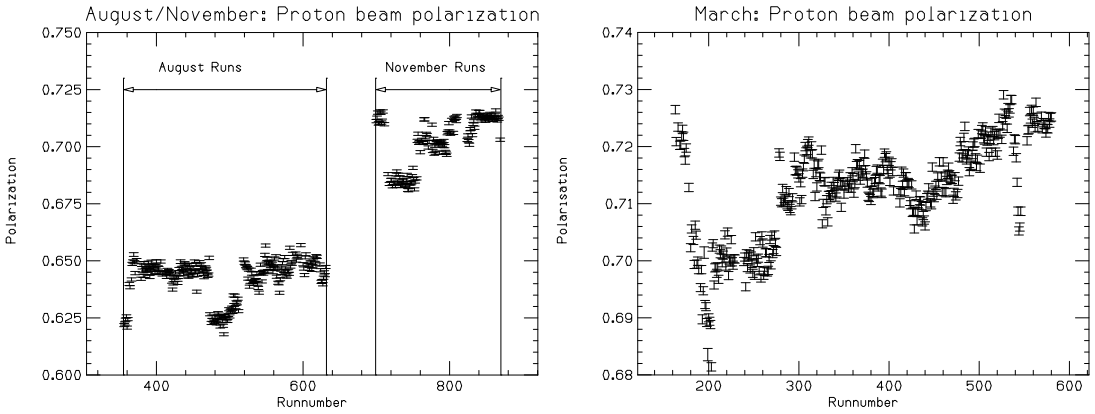

Figure 19: Proton beam polarization for all beam times

These average polarizations are multiplied with the spin transfer ratio for the $d(\vec{p},\vec{n})pp$ reaction at 0° as mentioned at page 19 to calculate the neutron polarization.

So the average polarizations for the several beam times are as follows

Exp.Run	$\vec{p}$ Pol. $\pm\Delta$ (%)	$\vec{n}$ Pol. $\pm\Delta$ (%)
August 98	65.5±0.1	30.1±0.15
November 98	70.5±0.1	32.5±0.15
March 99	71.7±0.1	33.2±0.15

Table 1: Average beam polarizations for the different experimental runs

The individual polarizations that are used for each run set in the analysis are listed in table 7 in the appendix.

4.3 Target polarization

The relative polarization of the target is measured every 10min via the response of a NMR probe. The uncertainty of the temperature measurement is the main error of the determination of the absolute target polarization.

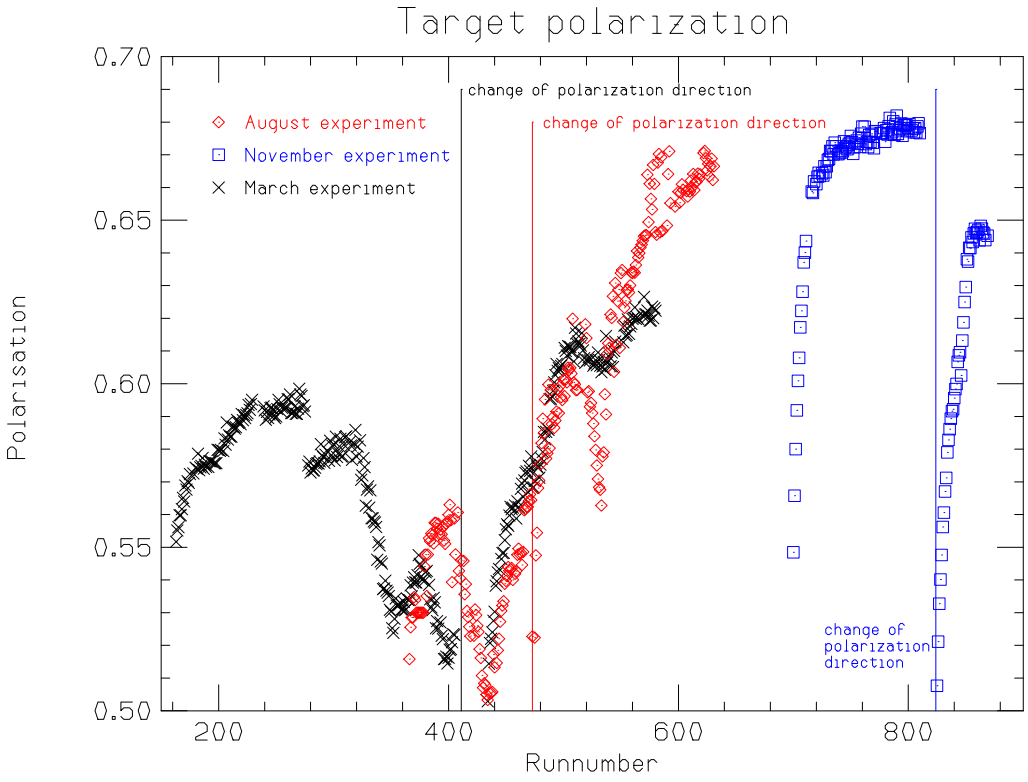

Figure 20: Target polarization for all beam times

The target is driven in the so called *spin-frozen-mode*. Thus the polarization is very stable over a long period of time. But as one can see from the histograms figure 20 there are some variations over the whole experiment due to fine tuning of the target crew and due to the polarization direction changes. On a long time scale there is a continuously increasing polarization, but the polarization does not change significantly during most runs or only in a very small range.

Therefore an average polarization for every run set can be taken. This is shown in table 7 in the appendix. Beam polarization is also included.

4.4 Neutron energy Distribution

As show in [25] the value for the spin transfer factor K_y^y of the neutron production reaction $d(\vec{p},\vec{n})pp$ at 0° depends on the energy of the outgoing neutron beam.

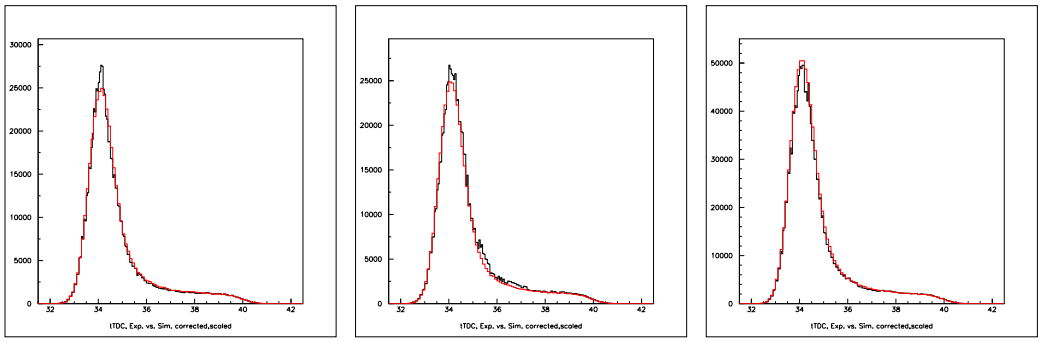

Figure 21: Experimental (black) and simulated (red) spectra for the 3 beamtimes

These values are measured to a very high accuracy in [3] and can be used to correct all experiments with a similar setup. This has been done and the theoretical calculations for the same setup as used in this experiment are discussed in [4]. The energy range of the 3 beamtimes for this experiment are in the same range and use the same targets. So one has to perform a Monte Carlo simulation with the values for each setup and compare the experimental target time spectra with the simulated ones as shown in figure 21. When applying the same cuts to the simulated spectra, one obtains the K_y^y values relevant for this experiment.

Also the spin rotation in the magnetic field right after the neutron production target is energy dependent. The maximum for the polarization distribution is in the experimental energy range, but one has to calculate the influence to the final polarization.

WFor the condition of the present experiment the results of these calculations are given in table 2 page 26.

Experiment	K_y^y	δp_x	δp_z
August 98	-0.413296	-0.018076	-0.999715
November 98	-0.415216	-0.017189	-0.999728
August 99	-0.414639	-0.017325	-0.999726

Table 2: Average Spin transfer and polarization distribution

4.5 False asymmetry corrections

Because the values of the asymmetry are small as compared to the overall sum of the rates, false asymmetry corrections are very important in this experiment. These concern mainly corrections for systematic shifts and differences between the two polarization states of the beam.

To reduce such false asymmetries the beam polarizations switches every 3 seconds. The solenoid field is also changed during the experiment to switch the orientation when turning the spin from y- to x-direction. In addition, the target spin direction is changed at least once per experiment runtime. Not more often, because it takes about 12–16h to switch from one maximum to the other.

First, the dead time of the electronics, which depends on the intensity of the beam, has to be corrected for. It is defined by

$$corr_d = \frac{d(\uparrow) - d(\downarrow)}{d(\uparrow) + d(\downarrow)} \quad with \quad d = 1 - \frac{trigger}{pretrigger} \tag{10}$$

with the trigger signals described in the electronics setup (page 16) and an electronically generated trigger as reference.

Also the Faraday cup, which is insensitive to beam position shifts, is compared with the target trigger, which gives an estimate about asymmetries from the beam which are called *false-asymmetries*.

$$corr_{false} = \frac{pf(\uparrow) - pf(\downarrow)}{pf(\uparrow) + pf(\downarrow)} \quad with \quad pf = \frac{protontrigger}{FaradayCup} \tag{11}$$

In addition there is an other point in the experimental setup, where we can compare beam asymmetries. This is the timing scintillator *(tisci)* located behind the carbon polarimeter. Usually this signal is used to optimize the width of the beam bunch. The signal is generated by elastic scattering on the carbon foil as mentioned on page 22 and collected in 2 Borer buffer spectra, interchanged by the polarization switch of the source. Because the beam is polarized in y-direction and the detector is located in y-plane, there is no asymmetry due to the polarization state. So we can calculate

$$corr_{tisci} = \frac{tf(\uparrow) - tf(\downarrow)}{tf(\uparrow) + tf(\downarrow)} \quad with \quad tf = \frac{\sum tisci}{FaradayCup} \tag{12}$$

The average correction values are shown in table 3.

The largest corrections result from dead time and the *tisci* beam correction. The dead time correction is independent of polarization states, so it represents an overall correction for all data. The correction from *tisci* and *false* are dependent on the polarization of the beam and therefore they affect the asymmetry. One also realizes, that the *false asymmetry* is small, but the *tisci* correction is in the same order as the dead time. So it is not negligible.

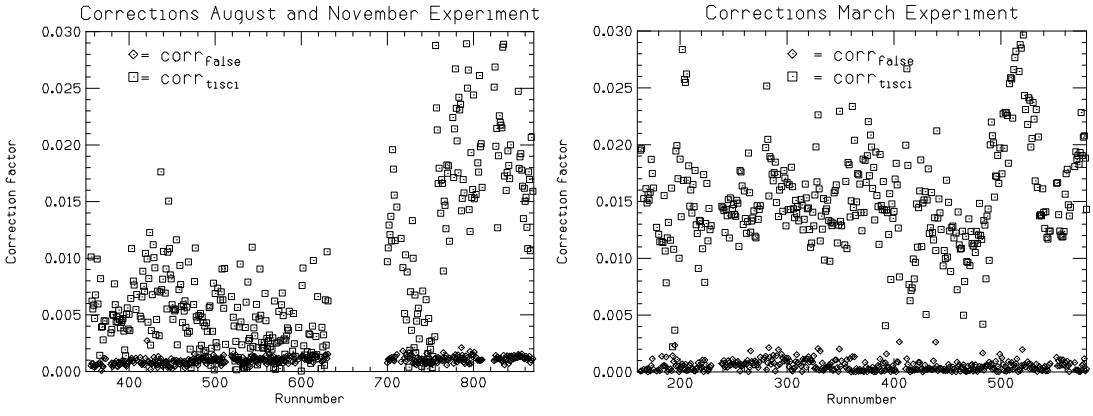

Figure 22: Corrections for the various beam times: corr_{false} and corr_{tisci}

One possible origin of the *false asymmetry* is a problem with the beam steering before the liquid deuterium target, because the correction based on the *false*

asymmetry is small, which means the FC sees more or less the same amount of beam for both polarization states, while the *tisci* observes a bigger rate in one polarization state. So one may suspect a change in the form of the beam spot when switching from one state to the other and a partial loss of beam on a collimator. This problem could be resolved by using the information of the secondary electron emission monitor (SEM), which has been done with the feedback loop program mentioned at page 12.

Experiment Run	Value (%)		
	$corr_d$	$corr_{false}$	$corr_{tisci}$
August 98	1.10±0.05	0.10±0.008	0.5±0.01
November 98	1.80±0.06	0.10±0.008	1.5±0.04
March 99	3.70±0.12	0.06±0.003	1.8±0.05

Table 3: Correction values

The other possibility would concern a problem with the ion source itself, i.e. a change of beam current depending on the polarization state. As pointed out in the proton polarization section page 17 this seems to be the correct hypothesis. But in this case it is not possible to correct in the beam line during the experiment — like the beam adjustment based on the SEM information mentioned above — but by the correction calculated in table 3 when analyzing the data. Because the *false* correction is included in *tisci*, the corrections applied on the experimental data are the *deadtime* and *tisci* correction.

4.6 Background

As one can see in figure 17 the remaining background comes from accidental (labeled as 1) events right under the peak (labeled as 3). Analysis shows that this background is uniform over the whole range (1) and unpolarized.

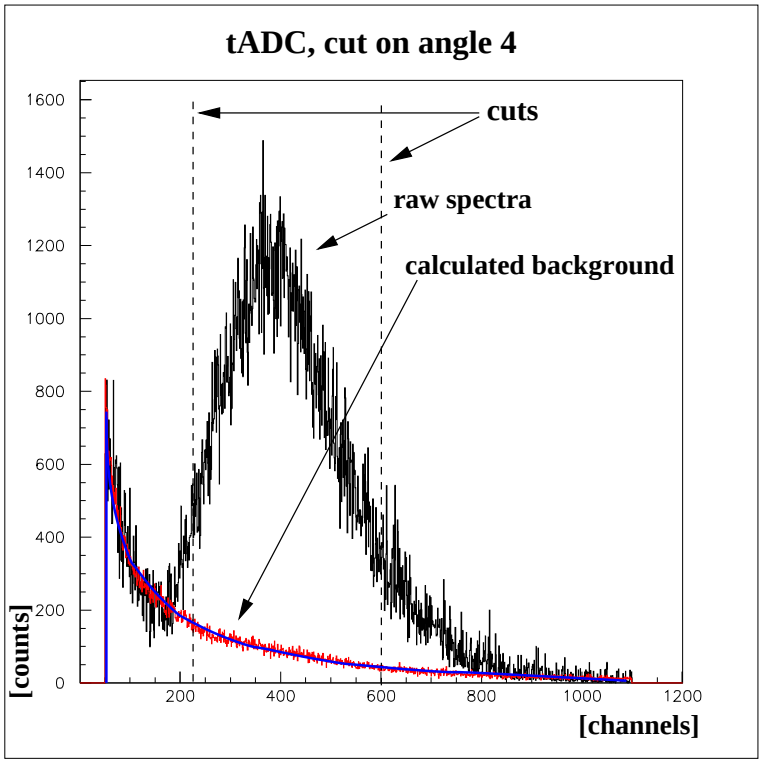

Figure 23: Target ADC, Angle 4 with background

To describe the shape of the background, cuts on the background 50 channels left and right of the signal peak (labeled as 3) summed and scaled to the first 50 channels of the histograms were used for the analysis. Then a fit is performed and the resulting background subtracted.

The spectra (figure 23) include the sum of both polarization states, the background and a fit of the background. With the overall and the background-subtracted (reduced) spectra one can calculate the ratio

$$corr_{bg} = \frac{N_{tot}}{N_{red}} \tag{13}$$

With this result the asymmetry is corrected by using

$$asym = \frac{N(\uparrow\uparrow) - N(\uparrow\downarrow)}{N(\uparrow\uparrow) + N(\uparrow\downarrow)} \cdot corr_{bg} \tag{14}$$

This method minimizes statistical errors which is important because of the small value of the asymmetry. The corr_{bg} is calculated for every run set and every angle. The resulting correction values for every angle and run set are listed in table 8.

5 Results

After applying all corrections, summing up the events and using equation (7), A_{zz} is extracted with

$$A_{zz} = \frac{1}{p_z^b}\frac{1}{p_z^t}\frac{N\uparrow\uparrow - N\uparrow\downarrow}{N\uparrow\uparrow + N\uparrow\downarrow} \tag{15}$$

where $N\uparrow\uparrow$ and $N\uparrow\downarrow$ are the number of events for spin parallel and antiparallel. Using the calculated polarizations for p_z^{beam} and p_z^{target} the resulting values for A_{zz} are listed in table 4

Angle (Θ_{cm})	A_{zz}	$\pm\Delta$
22.80°	0.1753	0.0069
28.60°	0.1557	0.0063
34.20°	0.1341	0.0050
39.90°	0.1262	0.0047
45.80°	0.0832	0.0042
51.60°	0.0547	0.0058
57.30°	0.0287	0.0063

Table 4: Experimental results for A_{zz}

The errors include the statistical errors and the following systematic errors:

Variable		source	Δ (%)
proton beam polarization	$p_{\vec{p}}^b$	measurement	0.1
target polarization	p_z^t	measurement	3.5
p - n spin transfer coefficient	K	other experiment	1.2

Table 5: Average errors for the different factors

These are the calculated error from the polarization measurement with the ^{12}C polarimeter, target polarization given by the temperature uncertainty at ∼100mK

as mentioned in the active target section on p.12 and the error for the proton – neutron spin transfer coefficient K_y^y as described in [2]. The errors for the inner angles (34.2°, 39.9°, 45.8° CM) are smaller than for the outer ones, as these angles correspond to the overlap area of the different runs and therefore had much higher statistics. Figure 21 shows the results of the present experiment together with the results by Zihlmann[1] and the PSA by Henneck[20]. The errors are remarkably small compared to the previous experiment. They also tend to lie below the line derived via the PSA.

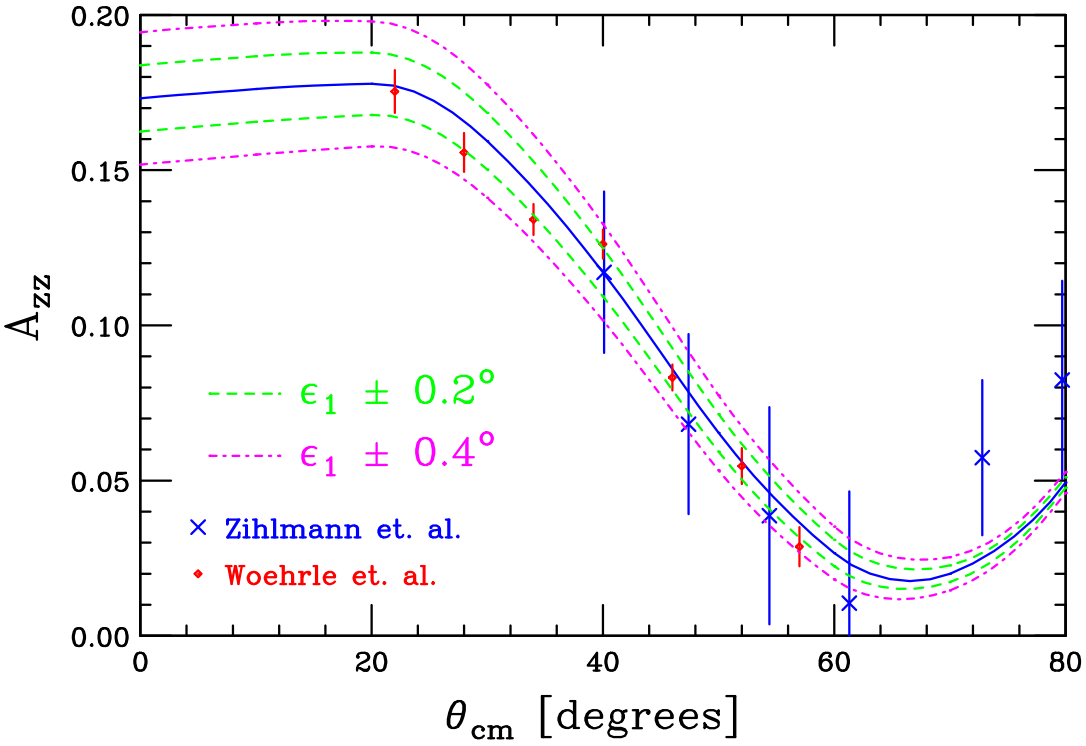

Figure 24: Resulting values of A_{zz}

6 Discussion

As shown in figure 24, the resulting data are in good agreement with the PSA for ϵ_1. In this picture are also included some curves for A_{zz} with values for $\epsilon_1 \pm 0.2°$

and $\epsilon_1 \pm 0.4°$. The data points lie within the variation of $\pm 0.4°$ with a slight tendency towards a greater value (lower lines).

Compared to all former experiments (see figure 2), the experimental values of the present experiment are able to define the value of A_{zz} and the ϵ_1 dependent variation to a higher precision.

7 Conclusion

The goal of this experiment is to measure A_{zz} with very high accuracy in an angular range where the influence of the $^1P_1$ phase is negligible. This also gives the possibility to improve other experimental values depending on A_{zz}, like the ones of A_{zx} measured in [4]. With these precise values it should be possible to improve the errors on A_{zx}. It should also be possible to perform a new PSA to extract ϵ_1 with a higher accuracy. All together it should be possible to extend significantly the knowledge on the tensor force of the NN-interaction in the low energy regime.

This experiment also involved participation in the development of a polarizable plastic scintillator and proved the usability of such an active target to suppress background, thus extending precise data to angles that were unreachable before.

A Spin $^1/_2$ on spin $^1/_2$ scattering

This appendix gives a brief overview on the underlying quantum mechanical formalism. A more detailed discussion can be found in [13] and [14].
A spin $^1/_2$ particle can be described by a Pauli spinor like

$$\Phi = \begin{pmatrix} a \\ b \end{pmatrix} \tag{16}$$

The expectation value of an hermitian operator describing an observable can be written as

$$\langle \Omega \rangle = \Phi^* \Omega \Phi = (a^*, b^*) \begin{pmatrix} \Omega_{11} & \Omega_{12} \\ \Omega_{21} & \Omega_{22} \end{pmatrix} \begin{pmatrix} a \\ b \end{pmatrix} \tag{17}$$

$$= |a|^2 \Omega_{11} + |b|^2 \Omega_{22} + 2Re(\Omega_{12} a b^*) \tag{18}$$

The equation (18) can also be interpreted as the trace of a matrix operation and we can express it as follows

$$\langle \Omega \rangle = Tr(\rho \Omega) \tag{19}$$

$$with \quad \rho = \begin{pmatrix} |a|^2 & ab^* \\ a^* b & |b|^2 \end{pmatrix} \tag{20}$$

where ρ is called density matrix and represents the ensemble of all particles in the beam. The effect of a scattering process of a single spin $^1/_2$ particle can be written as a linear function of final and initial state

$$\chi_f = M \chi_i \tag{21}$$

where M is a 2×2 matrix whith coefficients that are functions of energy and angle. When switching to more than a single particle, the scattering of a beam can be described by the density matrix of the ensemble. The relation between the initial and final state density matrix can be written as

$$\rho_f = M \rho_i M^\star = \frac{1}{2} M M^\star + \frac{1}{2} \sum_{j=x,y,z} p_j M \sigma_j M^\star \tag{22}$$

while using the density matrix of the initial state

$$\rho_i = \frac{1}{2}\left(1 + \sum_{j=x,y,z} p_j \sigma_j\right) \tag{23}$$

with σ_j, the Pauli spin matrices and p_j the polarization of the incoming particle. The differential cross section is

$$\frac{d\sigma}{d\Omega} = Tr\left(\rho_f\right) = Tr\left(M \rho_i M^\star\right) \tag{24}$$

with the polarization of the particles described by the expectation values of the Pauli spin matrix

$$p_{x,y,z} = \langle \sigma_{x,y,z} \rangle = \frac{Tr\left(\rho_f \sigma_{x,y,z}\right)}{Tr\left(\rho_f\right)} \tag{25}$$

Using the density matrix of the initial state (23) and equation (22)

$$\frac{d\sigma}{d\Omega} = Tr\left(\rho_f\right) = \underbrace{\frac{1}{2} Tr(MM^\star)}_{\frac{d\sigma_0}{d\Omega}} + \frac{1}{2} \sum_{j=x,y,z} p_j Tr(M \sigma_j M^\star) \tag{26}$$

and inserting

$$A_{x,y,z}(\theta) = \frac{Tr(M \sigma_j M^\star)}{Tr(MM^\star)} \tag{27}$$

where $A_{x,y,z}(\theta)$ is the analyzing power of the scattering process and $\frac{d\sigma_0}{d\Omega}$ the unpolarized differential cross section. one gets

$$\frac{d\sigma}{d\Omega} = \frac{d\sigma_0}{d\Omega}\left(1 + \sum_{j=x,y,z} p_j A_{x,y,z}(\theta)\right). \tag{28}$$

When replacing $Tr(\rho_f)$ with relation (25) and $Tr(MM^\star)$ with $\frac{d\sigma_0}{d\Omega}$ one ends up with

$$p_{x,y,z} \cdot \frac{d\sigma}{d\Omega} = \frac{d\sigma_0}{d\Omega}\left(P_{x,y,z}(\theta) + \sum_{j=x,y,z} p_j K_j^{x,y,z}(\theta)\right) \tag{29}$$

where $P_{x,y,z}$ is the overall polarization of the incoming beam and K_{out}^{in} is the spin transfer coefficient as function of the scattering angle θ.

B Polarizations

In this section we give the tables with the orientations and the values of the beam and target polarizations for the different data sets.

For the orientation: – means against flight direction of the beam, + means in flight direction. The solenoid does not turn the spin into the flight direction (*z direction*) (see figure 7) but orthogonal (*y direction*). But because the value of the solenoid (or the direction for the rotation) decides to which direction the spin will be turned by the dipole magnet behind the neutron production target, the value of the solenoid can be seen as the selection for the beam polarization.

For the determination of the direction of the beam polarization, also including the dipole magnet, see [4]. The target orientation is given by the magnetic field while polarizing and noted in the run book from the target operator of the PSI group.

Experiment Run	dataset Number	Target field orientation	Solenoid orientation	Run numbers (see run book)
August 98	Set 01	–	–	356–401
	Set 02	–	+	402–472
	Set 03	–	–	473–631
November 98	Set 04	+	+	700–711
	Set 05	+	–	716–800
	Set 06	+	+	801–810
	Set 07	–	+	824–869
March 99	Set 08	–	–	163–238
	Set 09	–	–	239–325

continued on next page

				continued from previous page
Experiment Run	dataset Number	Target field orientation	Solenoid orientation	Run numbers (see run book)
	Set 10	−	+	326–405
	Set 11	+	−	411–499
	Set 12	+	+	500–565
	Set 13	+	−	567–583

Table 6: Beam and target polarization directions for the different experimental runs

Given in the table are the average polarization values used for the analysis. The values do not change during a run and not significantly during a data set. Nevertheless these values are weighted with the number of events of a single run versus the sum of a run set. The numbers are absolute values and do not reflect the change of the polarization orientation as shown above, because this does not influence the final calculation of A_{zz} and therefore I did not list the signs as shown in table 6.

Exp.Run	dataset	tgt Pol. $\pm\Delta$ (%)	$\vec{n}$ Pol. $\pm\Delta$ (%)
August 98	Set 01	55.5±0.072	29.7±0.033
	Set 02	55.5±0.072	30.1±0.033
	Set 03	61.5±0.072	30.1±0.033
November 98	Set 04	60.5±0.072	32.6±0.033
	Set 05	65.5±0.072	32.5±0.032
	Set 06	65.5±0.072	32.8±0.033
	Set 07	62.5±0.072	32.5±0.033
March 99	Set 08	53.7±0.073	32.2±0.033
continued on next page			

continued from previous page

Exp.Run	dataset	tgt Pol. $\pm\Delta$ (%)	$\vec{n}$ Pol. $\pm\Delta$ (%)
	Set 09	58.5±0.072	33.0±0.033
	Set 10	58.5±0.072	32.7±0.034
	Set 11	55.5±0.072	33.2±0.034
	Set 12	61.5±0.072	33.2±0.034
	Set 13	62.5±0.072	34.3±0.035

Table 7: Average target and beam polarizations for the different experimental run sets

The values for the neutron polarization are average values calculated from the proton polarization. They are also without signs, because the polarization of the proton beam is switched every 3 seconds at the ion source and therefore it represents an average value of both polarization values. In this way the sign of the solenoid value shows the orientation of the spin (or the register in the hbook array of the data file).

C Background corrections

As described in section 4.6 the asymmetry of the counts (equation (14)) is multiplied with the ratio of background-corrected to background-noncorrected rates

These corrections are treated in the same way as the real signal. This means the same area from the peak as for the asymmetry calculation is selected for the calculations. One would expect that, because of the identical setup, they should be the same for the whole experiment. But because of the different electronics and calibrations in each experimental run they vary in fact. Within an experimental run the different data sets agree.

It is conspicuous that in the November run the background corrections are larger and in March significant lower. As the raw spectra look the same this seems to be a statistical effect, because each single data set in November (and August) is smaller in events and Megabytes compared to March.

Experiment Run	dataset Number	Scattering Angles 1	2	3	4	5
August 98	Set 01	1.16	1.26	1.18	1.18	1.35
	Set 02	1.19	1.26	1.20	1.27	1.33
	Set 03	1.20	1.26	1.21	1.31	1.35
November 98	Set 04	1.24	1.27	1.18	1.34	1.33
	Set 05	1.25	1.35	1.24	1.47	1.47
	Set 06	1.26	1.36	1.27	1.47	1.46
	Set 07	1.24	1.29	1.20	1.41	1.36
March 99	Set 08	1.18	1.10	1.07	1.14	1.10
	Set 09	1.17	1.10	1.07	1.13	1.09

continued on next page

continued from previous page

Experiment Run	dataset Number	Scattering Angles 1	2	3	4	5
	Set 10	1.17	1.10	1.07	1.14	1.10
	Set 11	1.18	1.10	1.06	1.14	1.09
	Set 12	1.17	1.09	1.06	1.13	1.08
	Set 13	1.17	1.09	1.06	1.12	1.08

Table 8: Background corrections for the individual run sets and angles

References

[1] B. Zihlmann, PhD thesis, University of Basel 1995.

[2] M. Zeier, PhD thesis, University of Basel 1996.

[3] M. Zeier et al. Polarization transfer in $^2H(\vec{p},\vec{n})pp$, *Nucl. Phys. A,* 654:541 1999.

[4] M. Hauger, PhD thesis, University of Basel 2002.

[5] B. van de6 Brandt, E.I. Bunyatova, P. Hautle, J.A. Konter, and S. Mango. *PSI Newsletter*, page 12 1994.

[6] P.A. Schmelzbach, ECR-Ionizer for intense polarized beams. *Proc. of int. workshop on polarized ion sources and polarized gas jets, KEK Tsakuba,* 1990.

[7] F. Hinterberger et al. Absolute analyzing power calibration in spin $^1/_2$ from spin 0 scattering. *Nucl.Inst. and Meth.*, A284:523-525 1989.

[8] P.D. Eversheim et al. Precise analyzing power calibration in proton – carbon scattering at 71MeV. *Phys. Lett. B,* 234:253-257 1990.

[9] P.R. Bevington and D. K. Robinson. Data reduction and error analysis in the physical sciences (2nd Edit.), *McGraw-Hill Inc., New York* 1992.

[10] R.J.N. Phillips. Comparison of p-p and n-n final state interaction. *Nucl. Phys.,* 35:650 1994.

[11] M.A. Pickar et al. 0° polarization transfer in $^2H(\vec{p},\vec{n})pp$ at 54 and 71MeV. *Phys. Rev. C,* 42:20-29 1990.

[12] T. Ericson and W. Weise. Pions and nuclei *Oxford science publications,* 1988.

[13] D. Fick. Einführung in die Kernphysik mit polarisierten Teilchen, *Bibliographisches Institut,* 1970.

[14] G.G.Ohlsen. Polarization transfer and spin correlation experiments in nuclear physics. *Rep.Prog.Phys.*, 35:771-801 1972.

[15] W.N. Cottingham, M. Lacombe, B. Loiseau, J.M. Richard, and R. VinhMau. *Phys. Rev. D*, 8:800 1973.

[16] R. Machleidt. *Adv. in Nucl. Phys.*, 19:189 1989.

[17] M.M. Nagels, T.A. Rijken, and J.J. de Swart. *Phys. Rev. D*, 17:768 1978.

[18] B. van den Brandt, E.I. Bunyatova, P. Hautle, J.A. Konter, and S. Mango. The PSI 100cm^3 frozen spin target *Nucl. Instr. and Meth. A*, 356:36 1995.

[19] M. Hammans et al. Neutron-proton spin-correlation parameter A_{zz} at 68 MeV. *Phys. Lett. B,* 66:2293 1991.

[20] R. Henneck. Phase shift analysis of NN scattering below 160MeV: Indication for a strong tensor force. *Phys. Rev.C,* 47:1859 1993.

[21] B. van den Brandt, E.I. Bunyatova, P. Hautle, J.A. Konter, and S. Mango. Polarized scintillator targets *Nucl. Instr. and Meth. A,* 446:592-599 2000.

[22] T.O. Niinikoski and F. Udo. Frozen spin polarized target. *Nucl. Instr. and Meth.,* 134:219-233 1976.

[23] T.J. Schmugge and C.D. Jeffries. *Phys.Rev.,* 138A:1785 1965.

[24] B. van den Brandt, P. Hautle, J.A. Konter. Progress in scintillating polarized targets for spin physics. *Proc. of the GDH 2002 conference*, Genova 2002.

[25] R. Henneck et al. Facility for 30-70MeV monoenergetic polarized neutrons. *Nucl.Inst. and Meth. A,* 259:329-340 1987.

[26] J. Binstock and R. Bryan. Nucleon-nucleon scattering near 50MeV. II. Sensitivity of various observables to the phase parameters. *Phys. Rev. D,* 9:2582 1974.

[27] R.B. Wiringa and V.G.J. Stoks and R. Schiavilla. Accurate nucleon-nucleon potential with charge-independence breaking. *Phys. Rev. C,* 51:38-51 1995.